CORA Cork Open Research Archive
Cartlann Taighde Oscailte Chorcaí

Title	Design and hybrid control of a two-axis flexure-based positioning system
Authors	Petri, Elena;Hao, Guangbo;Kavanagh Richard C.
Publication date	2021-03-07
Original Citation	Petri, E., Hao, G. and Kavanagh R. C. (2021) 'Design and hybrid control of a two-axis flexure-based positioning system', International Journal of Intelligent Robotics and Applications. https://doi.org/10.1007/s41315-021-00162-7
Type of publication	Article (peer-reviewed)
Link to publisher's version	10.1007/s41315-021-00162-7
Rights	© 2021, the Authors, under exclusive licence to Springer Nature Singapore Pte Ltd. part of Springer Nature. This is a post-peer-review, pre-copyedit version of an article published in International Journal of Intelligent Robotics and Applications. The final authenticated version is available online at: https://doi.org/10.1007/s41315-021-00162-7
Download date	2026-11-05 07:48:49
Item downloaded from	https://hdl.handle.net/10468/11201

UCC
University College Cork, Ireland
Coláiste na hOllscoile Corcaigh

Design and hybrid control of a two-axis flexure-based positioning system

E. Petri[1,2], G. Hao[2,*], R. C. Kavanagh[2,*]

[1]Department of Management and Engineering, University of Padova, Vicenza, Italy

[2]School of Engineering, University College Cork, Ireland

*Corresponding author

Abstract

In this paper, an accurate, large range, two-axis compliant positioning system is described and the performance of the implemented control system is analysed. The characteristics of two independently controlled axes are designed to be nominally identical and orthogonal. Both the kinematic and the kinetostatic cross-coupling interactions between the axes are statically analysed. The movement of each system axis can be modelled with linear equations when assuming a small motion range, upper bounded by about 0.2 mm. To achieve high-performance over the full permissible motion range (i.e., for movements up to ± 1 mm), the non-linearity due to stiffness has been considered and modelled to implement the controller. The control system is based on both a PID feedback controller and a force feed-forward controller based on a non-linear model. For sinusoidal or triangular reference signals, a repetitive controller (RC) based on a linear system model is added in parallel to improve system performances. Various dynamic tests have been performed, and the obtained simulation and experimental results are discussed. A suitable application of the designed RC is shown to significantly improve the accuracy of the system especially at the higher frequencies selected, thus allowing the accurate tracking of movements up to 50 Hz. The adopted encoder (with a resolution of 5 nm) allows the relative accuracy of the system to be of the order of a few percent for displacements of up to ±1 mm from the null position.

Keywords: positioning system, compliant mechanism, hybrid control, repetitive control

1. Introduction

Micropositioning and nanopositioning systems are mechatronic motion systems capable of micrometric or nanometric motion quality, in terms of precision, accuracy and resolution. Consequently, both the component choice and the manipulator design require very careful consideration. Flexure structures, such as compliant mechanisms, are utilized in most state-of-the-art high-performance positioners. In a compliant mechanism, at least part of the movement is

performed by exploiting the deflection of its flexible components. Compared to traditional rigid-body mechanisms, compliant mechanisms have several advantages, among which are [1]: reduced number of components (with reduced manufacturing and assembly time, and reduced cost), less movable joints or jointless structures (with consequent reduction of both wear and need of lubrication). Moreover, the mechanism precision is increased because backlash is reduced or eliminated. In addition, compliant mechanisms are easily miniaturized and they usually weigh less than their rigid-body counterparts.

Applications of micro-/nano-positioners include super-resolution microscopes, micromanipulation, lithography, scanning probes microscopes, biological cell manipulation and surface profilometry [2]-[7]. A critical application is the scanning probe microscope, in particular the Atomic Force Microscope (AFM) [8]-[12], where periodic reference signals (e.g. triangular signal in AFM) are used to drive an axis of the system.

Reference [13] reported a multi-axis, decoupled compliant parallel manipulator with a compact and symmetric configuration, which is suitable for micro-/nano-positioning applications with a range of travel of ±1 mm from the null position. Its kinetostatic analytical and experimental models have been described in detail. However, its multi-axis dynamic precision remains unknown, which is therefore the focus of this paper. This paper contributes to the system-level integration of such a multi-axis positioning system, including the control system hardware set-up, control methods, and dynamic tests.

Many high-performance positioning systems are actuated using piezo-electric actuators [12], [14]-[17]. However, the main drawback of such actuators is their limited motion range. To guarantee a large motion range (for example of the order of millimeters) actuation is performed using electromagnetic actuators [2],[18],[19] or voice coil (VC) actuators [3]-[6],[20]-[23]. In this paper, the latter approach is employed, because of both the large range of motion and the linear relation between input current and output force, thereby simplifying the control design. Moreover, voice coils actuators are frictionless, hysteresis-free and cog-free.

Various techniques have been implemented to control high-performance positioning systems. Most proposals reported in the literature are based on the flexure mechanisms. For example, in [6] and

[20] a Sliding Mode Control (SMC) with a PID controller is used, while in [21] a PID controller with a cross-coupled control and an Iterative Learning Control (ILC) based on zero-phase filtering, are proposed. A discrete time adaptive extended observer with exponential forgetting factor is adopted in [16], while an Enhanced Model-Predictive Control (EMPC) is implemented in [23]. Various papers adopt a control system based on a PI or a PID controller [3]-[5]. In some systems, the feedback control is implemented, together with a feed-forward controller. For example, a lead-lag type feedforward compensator is used in [18], while an inverse Preisach-model-based feedforward sliding-mode controller is proposed in [2].

The control algorithm proposed in this paper is based on a PID position feedback controller with added force feedforward. This latter component is based on a theoretical expression of the force required to perform a given movement, specified in terms of position, velocity and acceleration. In this way, the feedback controller, whose action is slower than the feedforward one, is required to compensate only for the difference between the real system and the theoretical equation, thereby improving the system's accuracy and dynamic performance. The compliant system shows a non-linear stiffness. Specifically, the relationship between force and position shows a significant cubic term related to the deformation of the compliant mechanism, as described in [24]. In the system described in this paper, this can be neglected only when the movement is smaller than 0.2 mm. Significant non-linear stiffness has been already reported in the literature [7], [25]. The force equation used in the feedforward controller considers the stiffness non-linearity. Thus, it allows the compensation of the non-linear system behaviour over the full operational motion range, thereby simplifying the design of the feedback controller. To the best of the authors knowledge, the use of this non-linear stiffness model to control the feedforward force has not reported in the literature to-date. The experimental results show that this simple approach provides a good compensation of such system non-linearities.

In multi-axis positioning systems, the cross-coupling interaction between the axes can negatively affect the system tracking. This effect requires analysis and, if necessary, compensation [6], [8], [21], [22], [26], [27]. The dynamic system performance is evaluated using periodic signals, such as sinusoidal or triangular signals [2], [18], [20], [25]. However, using technique specifically designed for periodic signals, such as repetitive control (RC) [9], [11], [15], [27], [28], or iterative learning control (ILC) [18], [21] can provide significant performance improvement. The designed RC is based

on a second order linear model of the system, thus enabling a simple implementation. Despite its simplicity, it provides good performance improvement for the non-linear system analysed. Compared to the controllers for flexure mechanisms reported in those papers listed above, the control strategy applied in the proposed system facilitates high-bandwidth, periodic movements of high accuracy, over a wide motion range.

The paper is organized as follows: in Section 2, the overall system is described, together with all its components, and the non-linear equation describing the system stiffness is reported. Moreover, both the kinematic and kinetostatic cross-coupling are statically analysed. The proposed control approach is described in Section 3. In Section 4, the simulated and experimental results obtained in dynamic operating condition are reported. Finally, some concluding remarks are presented in Section 5 of this paper.

2. System description

A two axes compliant positioning system, shown in Fig. 1, is considered. It is composed of two nominally identical orthogonal axes, each allowing a high-quality movement in a ±1 mm motion range. The mechanical structure is composed of three main parts: a compliant basic parallelogram mechanism (CBPM) for guiding the actuator in each axis (as described in [24]), the XYZ compliant parallel manipulator (CPM) shared between the axes (described in [13]), and a base frame.

The XYZ CPM, the structure of which is shown in Fig. 2, was designed using distributed-compliance wire beams, with a fully-symmetric (but the least over-constraints), compact and decoupled structure, so that each axis can be controlled separately using the same control strategy [13]. The wire flexures used in Fig. 2 are subject to spatial deflections. X and Y axes of the XYZ CPM were actuated in this paper to demonstrate the two-axis control system and method. The XYZ CPM as described in [13] can provide actuation isolation for guiding relatively low-weight actuators. However, to use large-force (i.e. high-weight) VC actuators for universal utilization, two separate CBPMs were added to the XYZ CPM to enable a capable guiding of the two actuators. Indeed, the CBPM component has been added to further constrain the motion of the voice coil actuator in the non-axial/non-desired direction, so avoiding possible actuator damage. In addition, this component increases the system's overall stiffness (i.e. natural frequency). As demonstrated in [13], the lost motion between the input and output in each axis of the XYZ CPM is trivial, and can be neglected in this paper, thus simplifying the system hardware design. Therefore, only a single-axis displacement

sensor (i.e. linear encoder) is used to measure the input displacement of the VC actuator of a particular axis. As shown in Fig.1, the encoder is installed on the CBPM component. Because the stiffness between the CBPM and the XYZ CPM is much bigger than that of the compliant mechanism itself, the encoder output provides an accurate representation of component of the displacement of the XYZ CPM in the direction of the CBPM movement. Thus, the encoder acts as a feedback sensor of the positioning system.

All these components utilize Aluminium 6061 (Young's Modulus E = 69000MPa). Each axis includes a servo amplifier (B25A20 by Advanced Motion Control) in current-loop mode, a voice coil actuator VCA (model LA30-48-000A manufactured by BEI Technologies INC) and an optical linear encoder (SI-HN-4000-01-0-FN-403-003-3, readhead number SRO15A, by Renishaw). The physical system is connected to a computer through a dSPACE DS1104 R&D Controller Board. The control program, implemented in Matlab/Simulink, was uploaded on the controller board using the dSPACE ControlDesk 5.4 software. The block diagram of one system axis, with all the components and their connections, is shown in Fig. 3.

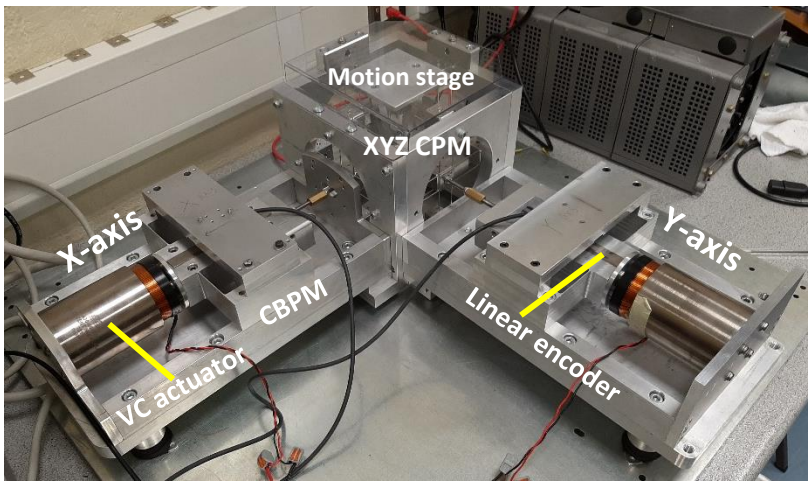


Fig. 1: The implemented two axes high-performance positioning system.

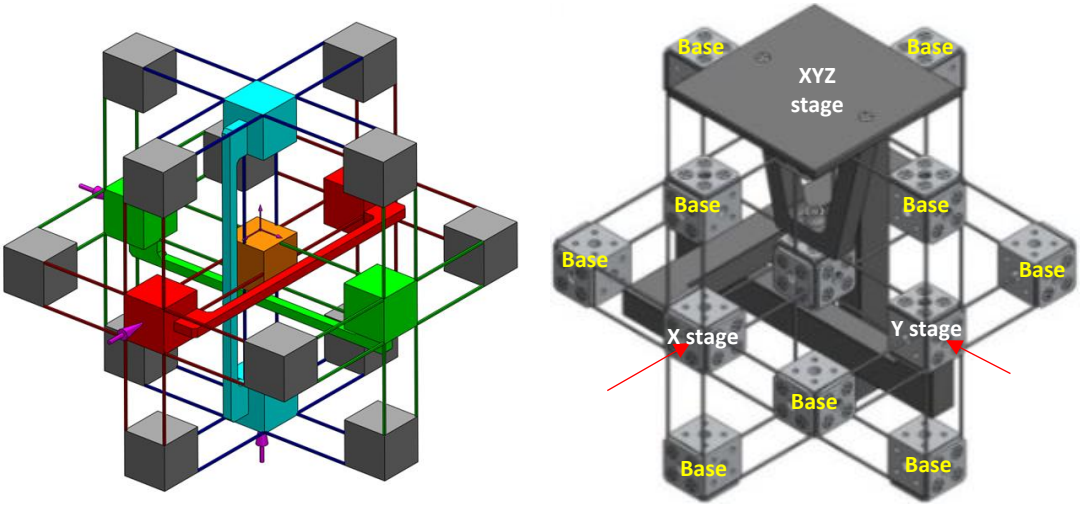


Fig. 2: XYZ CPM design: (a) Monolithic CAD design with three axis highlighted (grey colour indicating base stages); (b) Assembled design with the two controlled axes highlighted [13].

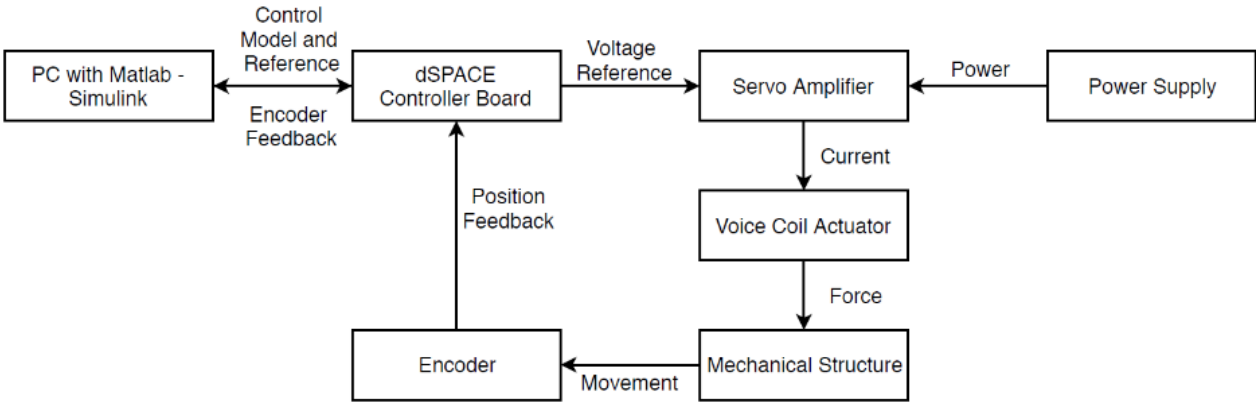


Fig. 1: One axis block diagram.

The mechanical system exhibits a non-linear behaviour mainly due to the stiffness non-linearity of the CBPMs. According to [29], the stiffness non-linearity can be neglected in a motion range of ±0.2 mm. Under that assumption, a mass-spring-damping model, (second order linear transfer-function) is sufficient for each axis. Thus, the ratio between the position signal measured by the encoder and the input voltage (from the DAC on the dSPACE controller board) can be written as [28]:

$$\frac{X(s)}{V(s)} = \frac{K_f K_d}{s^2 m_{tot} + sc + k_t} \tag{1}$$

where: K_f is the force sensitivity of the actuator, K_d is the servo amplifier gain, m_{tot} is the axis total mass, c is the axis viscous damping coefficient and k_t is the axis stiffness. Since $m_{tot} = 1.824$ Kg

and $k_t = 129460$ N/m, the resultant first resonant frequency is $f_r = 42.4$ Hz [28]. The bode diagram of Eq. (1) is shown in Fig. 4. As expected, the plots show a second order behaviour, with a DC gain equal to $20\log_{10}\frac{K_f K_d}{K_t} = -66.2\,dB$ and a resonant frequency at 42.4 Hz, with a corresponding peak of −39.4 dB. At higher frequencies, the magnitude of the transfer-function decreases with a decay rate of -40 dB/dec, while its phase approaches -180°. Thus, particular attention is required for reference signals with frequencies near the resonant frequency. Moreover, frequencies higher than the resonant frequency may require a very high input voltage to produce a significant movement.

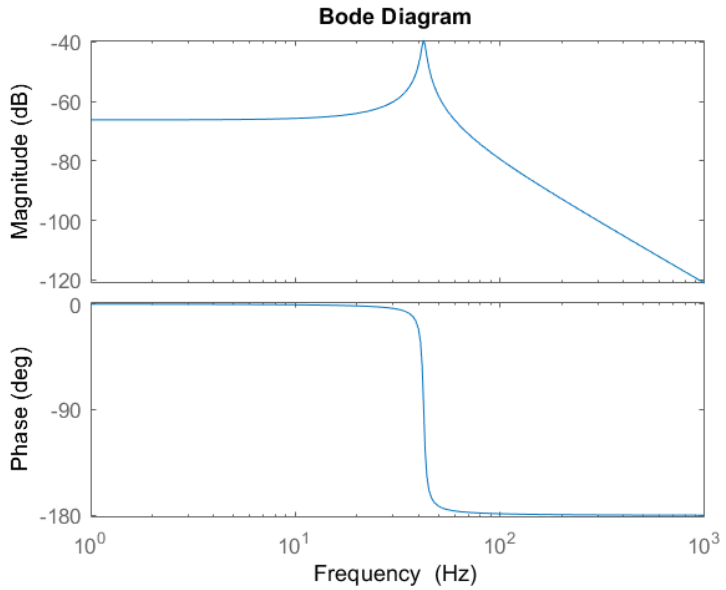


Fig. 2: Linear model Bode diagram

To exploit the full motion range of ± 1 mm, the non-linear equations of the CBPM primary actuation force and stiffness are [19]:

$$F_{CBPM} = 48\frac{EI}{L^3}X + \frac{2.88EI}{\frac{L^5}{p} + \frac{L^3X^2}{700}}X^3 \tag{2}$$

$$K = \frac{dF_{CBPM}}{dX} = 48\frac{EI}{L^3} + \frac{8.64EIX^2}{\frac{L^5}{p} + \frac{L^3X^2}{700}} - \frac{5.76EIL^3X^4}{700\left(\frac{L^5}{p} + \frac{L^3X^2}{700}\right)^2} \tag{3}$$

where: X is the primary translational motion, E is the Young's modulus, I is the second moment of area of a rectangular cross-section, L is the beam actual length and $p = \frac{12}{(T/L)^2}$, with T being the beam in-plane thickness.

The feedforward controller is implemented by adding the CBPM non-linear force to the XYZ CPM force $F_{XYZ} = 24\frac{12EI_{XYZ}}{L_{XYZ}^3}\ X$ [29] (where I_{XYZ} and L_{XYZ} are the second moment of area and length of the identical square wire beams, respectively, in the XYZ CPM) and the contributions of velocity and acceleration.

By analysing the effect of the cross-coupling interaction between the axes, the system can be controlled as a decoupled structure. Both the kinematic and kinetostatic cross-couplings were statically analysed. The kinematic cross-coupling occurs when a movement of one axis produces an unwanted movement on the other axis. Conversely, the kinetostatic cross-coupling arises when the force needed to move one axis increases when the position of the other axis differs from the null position.

The kinematic cross-coupling analysis was performed by driving one axis with a static reference signal and measuring, in open-loop, the movement of the other axis. The data showing the effect on the X-axis, when positive movements were performed on the Y-axis is shown in Fig. 5, together with the corresponding linear and cubic fittings. Similar results were obtained when negative Y-axis movements were performed, or when the roles of axes were exchanged.

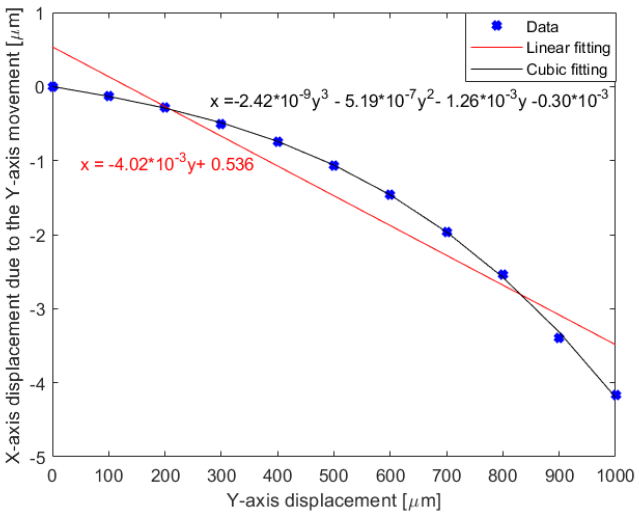


Fig. 3: Kinematic cross-coupling interaction on the X-axis when performing positive movements on the Y-axis.

Experimental results show that the shift introduced by the kinematic cross-coupling has a cubic behaviour and it is quite small (less than 1%) compared to the shift of the primary axis. A compensation of this effect using linear fitting of data was implemented. However, the compensation is found to be unnecessary for trajectories under closed-loop control, because the effect of the cross-coupling interaction was then so small that it was undetectable. Moreover, with dynamic reference signals (sinusoidal or triangular), the acquired data showed no appreciable difference when cross-coupling compensation was added. Thus, compensation of such cross-coupling will be neglected, henceforth.

In [30], the effect of the kinetostatic cross-coupling interaction in the actuation force was theoretically analysed. It was shown that the force needed to perform a movement on one axis increases if the other axis is not in the null position. Equation (4) shows the increment of the X-axis force ΔF_{XY} due to the kinetostatic cross-coupling with the Y-axis. Given the symmetrical nature of the system, effectively identical equations are relevant to both axes.

$$\Delta F_{XY} = \frac{EI}{L^3} \frac{1058400XY^2T^2}{(3X^2 + 3Y^2 + 175T^2)(3X^2 + 175T^2)} \tag{4}$$

where: X is the X-axis motion, Y is the Y-axis motion, while E, I, L and T are the same quantities as in (3). Due to symmetry, a similar equation holds when the axes are exchanged. In Fig. 6, the 3D plot of the X-axis force increment returned by (4) is shown. It is clear that the increase in actuation force is appreciable only when both axes are far away from the null position.

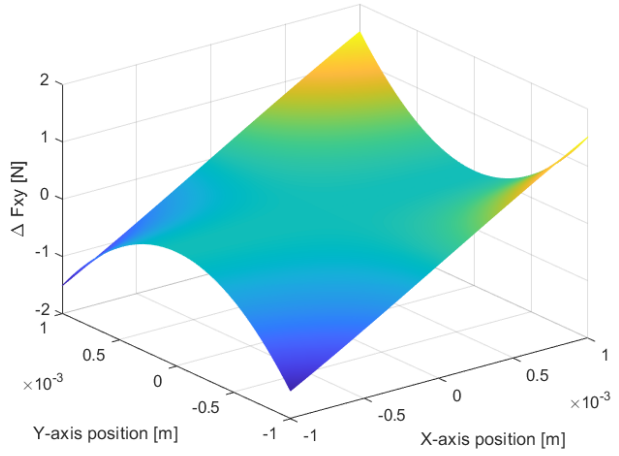


Fig. 4: X-axis force increment due to the kinematic cross-coupling with the Y-axis

The unwanted static, kinetostatic cross-coupling interaction was analysed experimentally using static signals. For this purpose, one axis was held in a fixed position, while the actuation force

needed to perform a desired movement on the other axis was measured and the force increment required to move one axis when the other is not in the null position was evaluated. Fig. 7 shows the force increment for the X-axis when the Y-axis was at +1 mm from the null position. Similar results were found when the Y-axis was held at ±0.5 mm and -1 mm, or when the roles of the axes were exchanged.

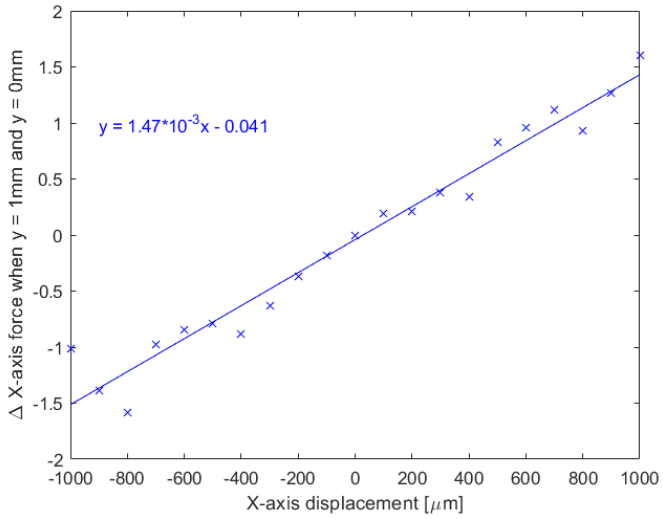


Fig. 5: X-axis force increment when the Y-axis was held in 1 mm from the null position.

It was verified that the variation in force is quite small in all the configurations chosen (around 1% in most cases). The effect of the kinetostatic cross-coupling was compensated by a linear fitting of static analysis data. However, no significant improvements were obtained when dynamic reference signals are used, since the system behavior is dominated by dynamic effects. Consequently, the kinetostatic cross-coupling effect will be neglected henceforth, because no such compensation is required.

3. Design of Controllers

Both axes of the system have the same structure and are controlled using the same control approach. Moreover, they are decoupled, so that they can be controlled independently.

Each axis control is composed by a feedback and a feedforward controller. The feedback controller increases the system's robustness to external noise or non-modelled effects. It is based on a PID approach, tuned with the *Ziegler-Nichols* method, as described in [31]. The feedforward controller is designed to improve the dynamic behaviour of the system, thereby reducing transient times.

When operating in the linear range (for movements up to ±0.2 mm), system performance significantly improves when the action of a force feedforward controller, based on Newton's law, is added to the PID feedback controller [32]. Thus, the feedforward output force is expressed in terms of the position, velocity and acceleration related to the reference trajectory:

$$F = m_{tot}\ddot{x} + c\dot{x} + k_t x \tag{5}$$

where: m_{tot} is the axis total mass, c is the axis viscous damping coefficient, k_t is the axis stiffness and x is the axis movement. When the axis movement is extended up to ±1 mm, (5) becomes:

$$F = m_{tot}\ddot{x} + c\dot{x} + k_t(x)x \tag{6}$$

where the term $k_t(x)x$ is the summation of the primary actuation force of the CBPM (2) and the XYZ CPM force F_{XYZ}. Both simulation and experimental results reported below show that implementation of the non-linear force feedforward (6) facilitates high-quality performance control over the full motion range.

In some applications of high-performance positioning systems, such as Atomic Force Microscopes (AFM) [8]-[11], periodic reference signals are used. In this case, system performance can be improved if a repetitive controller (RC) [9], [11], [15], [28] is added in the control scheme. The RC is intended to provide compensation of the periodic component of the tracking error and it requires a knowledge of both the period of the reference signal and the system's close-loop transfer-function. If, for the sake of simplicity, it is assumed that the system exhibits a predominantly linear behaviour, with closed-loop transfer-function $W(z) = B(z^{-1})/A(z^{-1})$, the RC transfer-function is [33]:

$$G_R(z^{-1}) = \frac{1}{1 - z^{-N}} K_R \frac{z^{-N+d+m} A(z^{-1})(z^{-m}B^-(z))}{B^+(z^{-1})b} \tag{7}$$

where: N is the number of samples in a single period, d is the relative degree of $W(z)$, m is the number of the zeros outside the unit radius circumference and K_R is the RC gain. In (7), the numerator polynomial of $W(z)$ is expressed as the product $B(z^{-1}) = B^+(z^{-1})\,B^-(z^{-1})$, where $B^+(z^{-1})$ corresponds to its stable zeros, while $B^-(z^{-1})$ relates to the unstable ones. Observe that $B^-(z^{-1})$ is not physically feasible, but $\left(z^{-m}B^-(z)\right)$ it is. Finally, $b \geq \max\left|B^-\left(e^{-j\omega}\right)\right|^2$ with $\omega \in [0, \pi]$. It has been shown in [32] that this controller is asymptotically stable if $0 < K_R < 2$.

A schematic representation of the control scheme implemented for each axis of the system is shown in Fig.8.

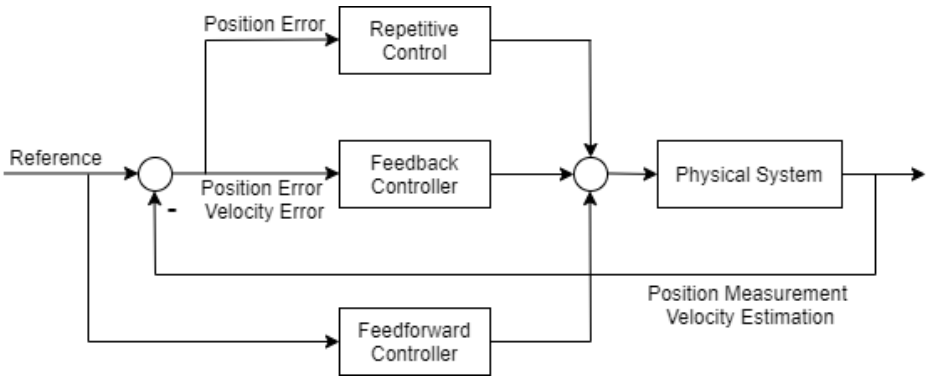


Fig. 6: Schematic control scheme

Observe that the feedforward controller uses position, velocity and acceleration reference inputs, while the feedback controller requires only position and velocity. Since only a position measurement is performed, system velocity is estimated through a suitable observer, as described in [31].

4. Simulation and experimental results

4.1 Simulation results

A number of simulations and experiments were performed using Simulink to assess the dynamic performance when feeding both axes with sinusoidal or triangular signals, but with different amplitude and frequency values. The analysis was performed both without and with RC. Simulation results are shown for only one axis because both axes are modelled identically, and the related control algorithms are decoupled. (Note that an addition at the system input of random noise about 1 µm amplitude to the nonlinear model was made because its contribution at the system output matched well the magnitude of the noise measured on the physical system.

Simulations showed that the RC action significantly reduces the position error, but that the error starts to increase after some time. Simulations showed that this undesired effect is due to system non-linearity, while the RC implementation is conversely based on a linear system model. However, if the RC action is terminated just before the error starts to increase, that detrimental behaviour is avoided, and a steady-state reduction ensues. The optimum termination time is easily found experimentally because it is repeatable and consistent for a particular type of periodic trajectory.

The results returned by some typical simulations are reported below. The position error corresponding to a sinusoidal reference signal of 500 µm amplitude and 10 Hz frequency is shown in Fig. 9. Results obtained without and with the RC action are shown and the related RMS errors are equal to 9.75 µm and 0.44 µm, respectively. The system's performance improvement due to RC is evident. It is worth observing that the position error signal exhibits a periodic behaviour at the frequency of the reference signal when RC is not implemented.

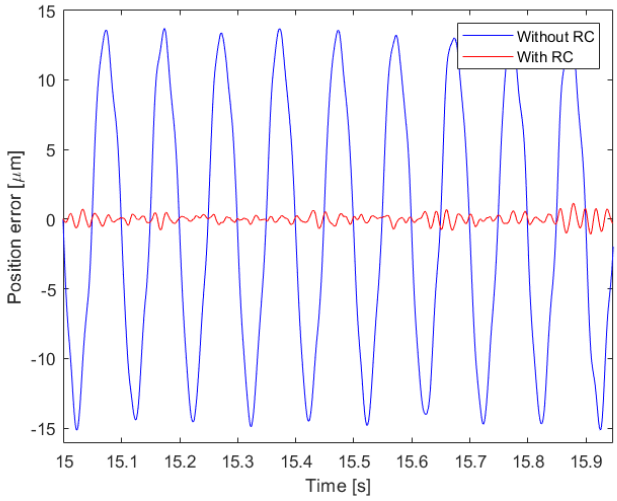


Fig. 7: Simulation results (both without and with RC action) for the position error corresponding to a sinusoidal reference signal of 500 µm amplitude and 10Hz frequency.

The same analysis was performed using a triangular reference signal with 500 µm amplitude and 10 Hz frequency. The corresponding position error obtained is reported in Fig. 10. The RMS errors of the results obtained both without and with the RC action are equal to 27.77 µm and 0.69 µm, respectively. Thus, the RC action strongly improves the system performance also in this case. As before, that the error still exhibits a periodic behaviour at the frequency of the reference signal when the RC is not used. Also, the error is significantly greater than the one observed with a sinusoidal reference signal, due to the first derivative discontinuity of the triangular wave.

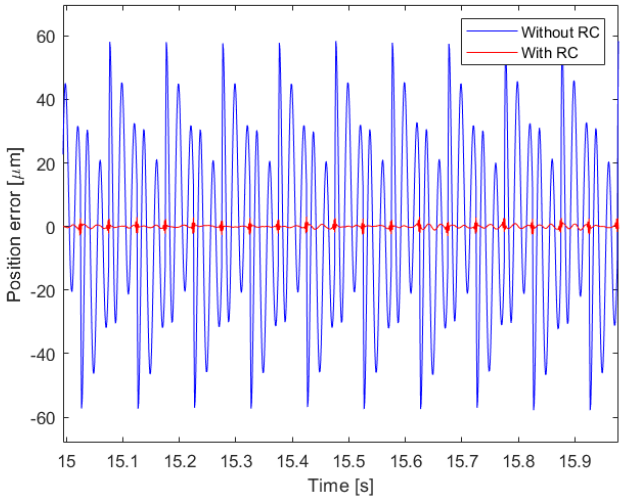


Fig. 8: Simulation results (both without and with RC action) for the position error corresponding to a triangular reference signal of 500 µm amplitude and 10Hz frequency.

4.2 Experimental results

Operating conditions similar to those considered in simulations were applied to the physical system. The obtained results are reported in the following. Sinusoidal or triangular reference signals were applied to both axes considering different values of amplitude and frequency. The Y-axis signal was phase-shifted by 90° with respect to the X-axis signal, in order to drive the system in such a way that circular or square shapes can be drawn in the XY-plane. All reference signal configurations considered were tested without or with the RC action, which was stopped when the error started to increase, as with the simulations.

The RMS position errors corresponding to sinusoidal reference signals are presented in Tables 1 and 2, for 100 µm and 500 µm amplitude, respectively and different frequencies. (The amplitude of the test was limited to 100 µm at 20 and 50 Hz due to the limitation of the available power supply). The position error waveforms for both axes are shown in Fig.11 when a sinusoidal reference signal of 500 µm amplitude and 10 Hz frequency is used. Fig. 12 shows the corresponding XY-plane plot.

Table 1: Experimental RMS position error for sinusoidal reference signal of 100 µm amplitude at different frequencies. Results obtained both without and with the RC action are shown.

Frequency [Hz]	1		5		10		20		50	
RC	NO	YES	NO	YES	NO	YES	NO	YES	NO	YES
RMSE X-axis [µm]	1.84	1.19	3.61	0.74	5.41	0.55	6.45	2.98	78.87	1.57
RMSE Y-axis [µm]	1.57	1.46	3.81	2.66	7.71	1.78	11.39	2.28	57.82	2.43

Table 2: Experimental RMS position error for sinusoidal reference signal of 500 µm amplitude at different frequencies. Results obtained both without and with the RC action are shown.

Frequency [Hz]	1		5		10	
RC	NO	YES	NO	YES	NO	YES
RMSE X-axis [µm]	2.50	1.46	8.20	0.29	16.69	1.54
RMSE Y-axis [µm]	1.74	1.34	6.95	3.52	19.88	1.39

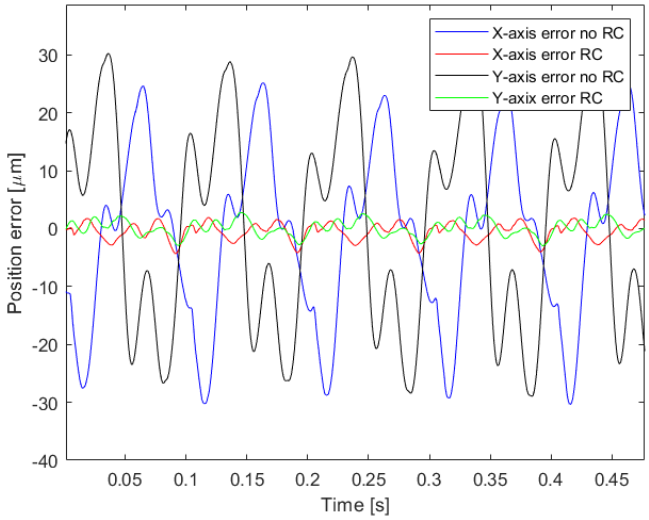


Fig. 9: Experimental results for the position error corresponding to a sinusoidal reference signal of 500 µm amplitude and 10Hz frequency on both axes. Results obtained both without and with the RC action are shown.

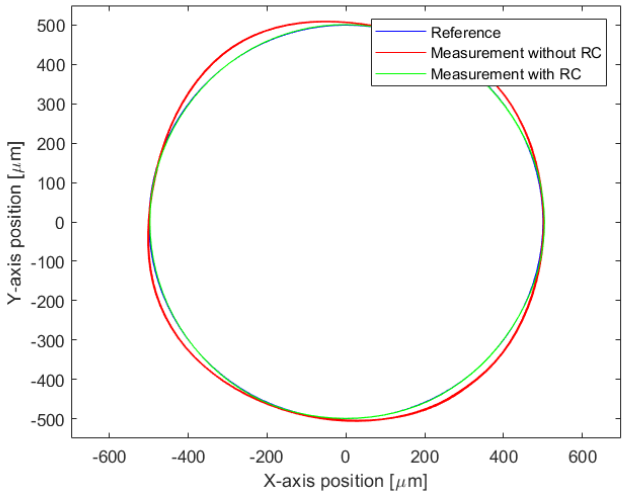


Fig. 10: XY-plane. Experimental plots related to quadrature sinusoidal reference signals with 500 µm amplitude and 10 Hz frequency on system axes.

Experimental data show that RC improves the system performance in all the chosen configurations. However, the improvement is bigger at the highest selected frequencies. As expected from simulations, Fig. 11 shows that the position error exhibits a periodic behaviour at the reference signal frequency when RC is not applied.

Similar configurations were tested using triangular reference signals with different amplitudes and frequencies. The obtained RMS position errors are reported in Tables 3 and 4 for 100 µm and 500 µm amplitude, respectively and for different frequencies. The position error waveforms for both axes are shown in Fig. 13 when a triangular reference signal of 500 µm amplitude and 10 Hz frequency is used. Fig. 14 shows the corresponding XY-plane plot.

Table 1: Experimental RMS position error for triangular reference signal of 100 µm amplitude at different frequencies. Results obtained both without and with the RC action are shown.

Frequency [Hz]	1		5		10		20		50	
RC	NO	YES	NO	YES	NO	YES	NO	YES	NO	YES
RMSE x-axis [µm]	1.90	2.90	3.82	4.35	6.04	2.50	9.21	3.01	64.78	2.97
RMSE y-axis [µm]	1.58	3.10	3.99	3.47	8.43	2.41	13.73	5.25	44.71	3.75

Table 2: Experimental RMS position error for triangular reference signal of 500 µm amplitude at different frequencies. Results obtained both without and with the RC action are shown.

Frequency [Hz]	1		5		10	
RC	NO	YES	NO	YES	NO	YES
RMSE X-axis [µm]	25.72	12.38	12.30	3.13	35.99	8.86
RMSE Y-axis [µm]	39.18	35.58	34.48	10.97	44.72	29.90

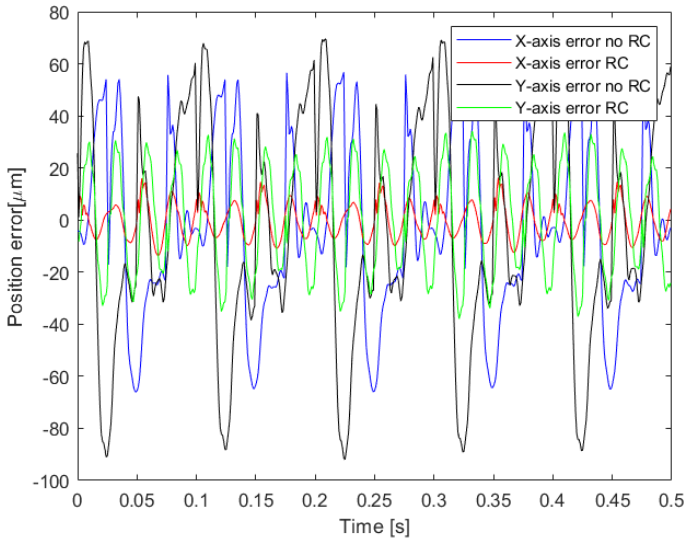


Fig. 11: Experimental results for the position error corresponding to a triangular reference signal of 500 µm amplitude and 10Hz frequency on both axes. Results obtained both without and with the RC action are shown.

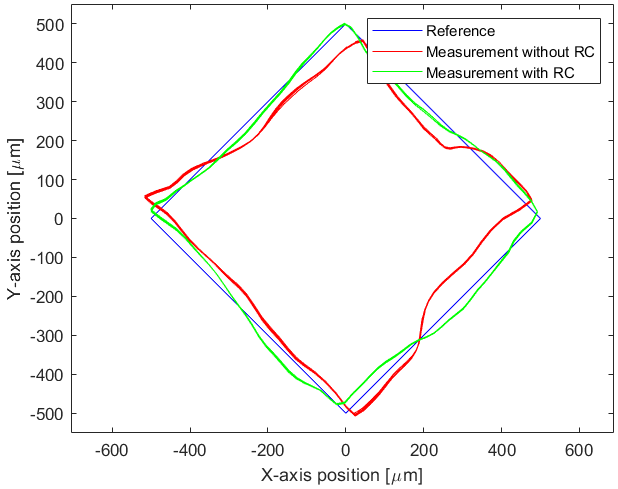


Fig. 12: XY-plane. Experimental plots related to quadrature triangular reference signals with 500 µm amplitude and 10 Hz frequency on system axes.

Experimental results showed that the inclusion of RC action was always advantageous for sinusoidal reference signals. For a triangular reference, it also improved performance except in the specific case of very small, low magnitude, low frequency (less than about 5 Hz) references, when the performance worsened, as shown in Table 3. Moreover, the tracking errors obtained with the triangular reference signals are bigger than those for the sinusoidal reference signals. As commented in the simulation section, this effect is due to discontinuity in the first derivative of the triangular wave.

5. Conclusions

In this paper, a description and analysis of a two-axis high-performance compliant positioning system have been presented, with emphasis on the control strategies utilized. It has been shown that the system exhibits a non-linear behaviour due to ~~a~~ stiffness non-linearity, which is not negligible when axis movement is larger than ±0.2 mm from the null position. This non-linear behaviour has been modelled and compensated for by means of a suitable control system.

Both kinematic and the kinetostatic cross-coupling interactions between the axes were statically analysed. It was verified that their effects are negligible in the presence of a controller that includes a feedback controller.

Finally, different dynamic testing were performed on sinusoidal or triangular periodic reference signals. Then, a suitable RC controller enabled significant performance improvement, particularly at

higher frequencies. Even without RC action, the system relative accuracy is in the order of few percent of the displacement amplitude up to 10 Hz with both sinusoidal and triangular required position reference signal of amplitude up to ±1 mm from the null position. When the RC is suitably activated, a significant improvement in system accuracy is obtained, except in the case of triangular reference signal with small amplitude and low frequency. The RC action was seen to facilitate accurate control of higher bandwidth position movements of up to 50 Hz.

System performances can be further improved by using lower noise servo amplifiers. Moreover, increasing the power provided by the supply system could enable higher frequency movement for either axis, over the full motion range. It is worth observing that the proposed control approach is beneficial for many similar systems which exhibit non-linear a stiffness or require the tracking of periodic trajectories.

References

[1] Larry L. Howell. Compliant mechanisms. Wiley, New York, 2001.

[2] Xiao, S., & Li, Y. (2012). "Optimal Design, Fabrication, and Control of an XY Micropositioning Stage Driven by Electromagnetic Actuators". *IEEE Transactions on Industrial Electronics*, *60*(10), 4613-4626

[3] Shang, J., Tian, Y., Li, Z., Wang, F., & Cai, K. (2015). "A novel voice coil motor-driven compliant micropositioning stage based on flexure mechanism". Review of Scientific Instruments, 86(9), 095001.

[4] Xu, Q. (2013). "Design and development of a compact flexure-based XY precision positioning system with centimeter range". *IEEE Transactions on Industrial Electronics*, *61*(2), 893-903.

[5] Kang, D., Kim, K., Kim, D., Shim, J., Gweon, D. G., & Jeong, J. (2009). "Optimal design of high precision XY-scanner with nanometer-level resolution and millimeter-level working range". Mechatronics, 19(4), 562-570.

[6] Al-Jodah, A., Shirinzadeh, B., Ghafarian, M., Das, T. K., Tian, Y., Zhang, D., & Wang, F. (2020). "Development and control of a large range XYΘ micropositioning stage". *Mechatronics*, *66*, 102343.

[7] Awtar, S., & Parmar, G. (2013). "Design of a large range XY nanopositioning system". *Journal of Mechanisms and Robotics*, *5*(2).

[8] Yong, Y. K., Liu, K., & Moheimani, S. R. (2009). "Reducing cross-coupling in a compliant XY nanopositioner for fast and accurate raster scanning". *IEEE Transactions on Control Systems Technology*, *18*(5), 1172-1179.

[9] Kenton, B. J., & Leang, K. K. (2011). "Design and control of a three-axis serial-kinematic high-bandwidth nanopositioner". *IEEE/ASME Transactions on Mechatronics*, *17*(2), 356-369.

[10] Tang, H., & Li, Y. (2013). "Development and active disturbance rejection control of a compliant micro-/nanopositioning piezostage with dual mode". *IEEE Transactions on Industrial Electronics*, *61*(3), 1475-1492.

[11] Necipoglu, S., Cebeci, S. A., Basdogan, C., Has, Y. E., & Guvenc, L. (2011). "Repetitive control of an XYZ piezo-stage for faster nano-scanning: Numerical simulations and experiments". *Mechatronics*, *21*(6), 1098-1107.

[12] Tian, Y., Cai, K., Zhang, D., Liu, X., Wang, F., & Shirinzadeh, B. (2019). Development of a XYZ scanner for home-made atomic force microscope based on FPAA control. *Mechanical Systems and Signal Processing*, *131*, 222-242.

[13] Li, H., & Hao, G. (2018). "Position-space-based design of a symmetric spatial translational compliant mechanism for micro-/nano-manipulation". *Micromachines*, *9*(4), 189.

[14] Polit, S., & Dong, J. (2010). “Development of a high-bandwidth XY nanopositioning stage for high-rate micro-/nanomanufacturing”. *IEEE/ASME Transactions on mechatronics*, *16*(4), 724-733
[15] Li, Y., & Xu, Q. (2011). “Design and robust repetitive control of a new parallel-kinematic XY piezostage for micro/nanomanipulation”. IEEE/ASME Transactions on Mechatronics, 17(6), 1120-1132.
[16] Chao, P., Han, C., Zou, J., & Zhang, G. (2016). “H [infinity] optimal inversion feedforward and robust feedback based 2dof control approach for high speed-precision positioning systems”. Journal of Control Science and Engineering, 2016.
[17] Rana, M. S., Pota, H. R., & Petersen, I. R. (2018). “A Survey of Methods Used to Control Piezoelectric Tube Scanners in High-Speed AFM Imaging”. Asian Journal of Control, 20(4), 1379-1399.
[18] Parmar, G., Barton, K., & Awtar, S. (2014). “Large dynamic range nanopositioning using iterative learning control”. *Precision engineering*, *38*(1), 48-56.
[19] Chen, M. Y., Huang, H. H., & Hung, S. K. (2009). “A new design of a submicropositioner utilizing electromagnetic actuators and flexure mechanism”. *IEEE Transactions on Industrial Electronics*, *57*(1), 96-106.
[20] Cai, K., Tian, Y., Liu, X., Zhang, D., Shang, J., & Shirinzadeh, B. (2019). “Development and control methodologies for 2-DOF micro/nano positioning stage with high out-of-plane payload capacity”. *Robotics and Computer-Integrated Manufacturing*, *56*, 95-105.
[21] Ulu, N. G., Ulu, E., & Cakmakci, M. (2016). “Design and analysis of a modular learning based cross-coupled control algorithm for multi-axis precision positioning systems”. *International Journal of Control, Automation and Systems*, *14*(1), 272-281.
[22] Lu, S., Tia, C., & Yan, P. (2019). “Adaptive extended state observer based synergetic control for a long stroke compliant micro stage with stress stiffening”. *IEEE/ASME Transactions on Mechatronics*.
[23] Xu, Q. (2011). “New flexure parallel-kinematic micropositioning system with large workspace”. *IEEE Transactions on Robotics*, *28*(2), 478-491.
[24] Hao, G., & Li, H. (2015). “Nonlinear analytical modeling and characteristic analysis of a class of compound multibeam parallelogram mechanisms”. *Journal of Mechanisms and Robotics*, *7*(4).
[25] Lu, S., Tia, C., & Yan, P. (2019). “Adaptive extended state observer based synergetic control for a long stroke compliant micro stage with stress stiffening”. IEEE/ASME Transactions on Mechatronics.
[26] Lee, C., Stepanick, C. K., Lee, S. K., & Tarbutton, J. A. (2016). “Cross-coupling effect of large range XY nanopositioning stage fabricated by stereolithography process”. *Precision Engineering*, *46*, 81-87.
[27] Zhang, Z., Yang, X., & Yan, P. (2019). Large dynamic range tracking of an XY compliant nanomanipulator with cross-axis coupling reduction. *Mechanical Systems and Signal Processing*, 117, 757-770.
[28] Eielsen, A. A., Gravdahl, J. T., & Leang, K. K. (2015). “Low-order continuous-time robust repetitive control: Application in nanopositioning”. *Mechatronics*, *30*, 231-243.
[29] Sandon, R., Li, H., Ferro, F., Trevisani, A., Kavanagh, R., & Hao, G. (2017). “High-Performance Control of a Single-Axis Compliant Nano-Positioning System: Design”. *Proceedings of the 34th International Manufacturing Conference.*
[28] Li, H. (2016). “Approaches to the synthesis, modelling and optimisation of spatial translational compliant parallel mechanisms”. PhD thesis, University College Cork.
[29] Marchi, A. (2019). “Wide Range Control and Performance Evaluation of a Single-Axis Compliant Nano-Positioning System”. Master Thesis, University of Padua.
[30] Sandon, R., Li, H., Ferro, F. F., Trevisani, A., Hao, G., & Kavanagh, R. (2017). “High-Performance Control of a Single-Axis Compliant Nano-Positioning System: Control”. *Proceedings of the 34th International Manufacturing Conference*.
[31] Tomizuka, M., Tsao, T., and Chew, K. (1989). “Analysis and Synthesis of Discrete-Time Repetitive Controllers”. ASME. *J. Dyn. Sys., Meas., Control*. September 1989; 111(3): 353–358.